A critique of Emanuel's hurricane model and potential intensity theory

Roger K. Smith,[a]* Michael T. Montgomery[b] and Stefanie Vogl[a]

[a] *Meteorological Institute, University of Munich, Munich, Germany*
[b] *Dept. of Meteorology, Naval Postgraduate School, Monterey, CA and NOAA's Hurricane Research Division, Miami, FL, USA*

ABSTRACT: We present a critique of Emanuel's steady-state hurricane model, which is a precursor to his theory for hurricane potential intensity (PI). We show that a major deficiency of the theory is the tacit assumption of gradient wind balance in the boundary layer, a layer that owes its existence to *gradient wind imbalance* in the radial momentum equation. If a more complete boundary-layer formulation is included using the gradient wind profiles obtained from Emanuel's theory, the tangential wind speed in the boundary layer becomes supergradient, invalidating the assumption of gradient wind balance. We show that the degree to which the tangential wind is supergradient depends on the assumed boundary-layer depth. The full boundary-layer solutions require a knowledge of the tangential wind profile above the boundary layer in the outer region where there is subsidence into the layer and they depend on the breadth of this profile. This effect is not considered in Emanuel's theory. We argue that a more complete theory for the steady-state hurricane would require the radial pressure gradient above the boundary layer to be prescribed or determined *independently* of the boundary layer.

The issues raised herein highlight a fundamental problem with Emanuel's theory for PI, since that theory makes the same assumptions as in the steady-state hurricane model. Our current findings together with recent studies examining intense hurricanes suggest a way forward towards a more consistent theory for hurricane PI. Copyright © 2008 Royal Meteorological Society

KEY WORDS   tropical cyclone; typhoon; boundary layer; friction layer; gradient wind balance

Received 7 November 2007; Revised 2 March 2008; Accepted 4 March 2008

1. Introduction

In the first of what has turned out to be a series of very influential papers, Emanuel (1986, henceforth E86) presented a steady axisymmetric model for a mature hurricane. We consider this paper to be an important milestone in tropical cyclone research in that it re-focussed attention on the importance of the radial gradient of sea surface moisture fluxes in the storm-scale energetics. The hurricane model described therein was a prelude to the development of an axisymmetric theory for the potential intensity (PI) of a tropical cyclone, which we refer to as EPI-theory (Emanuel, 1988; Emanuel, 1995; Bister and Emanuel, 1998). Since its inception, EPI-theory has been called upon by many researchers as a standard for comparison with the intensity attained in numerical models (e.g. Frank and Ritchie, 2001; Persing and Montgomery, 2003) or assessments of possible changes in the intensity of hurricanes as a result of global warming (e.g. Knutson and Tuleya, 2004; Emanuel, 2005; Bengtsson *et al.*, 2007). At the present time it appears to be the only such theory of merit for these applications (Camp and Montgomery, 2001). Even so, there are indications that the theory is deficient. For example, Persing and Montgomery (2003) have shown that high-resolution numerical models have a tendency to produce 'superintense' storms, superintense meaning that they significantly exceed the intensity predicted by EPI-theory. Moreover, the calculated PI depends sensitively on the assumed relative humidity at the radius of maximum tangential wind speed, which Emanuel generally takes to be 80%. In this paper we draw attention to a fundamental inconsistency of the hurricane model and of EPI-theory, namely the assumption of gradient wind balance in the boundary layer, both inside and outside the radius of maximum tangential wind speed. The consequences of this assumption for Emanuel's hurricane model and EPI-theory are discussed below and a way forward is sketched.

This paper is organized as follows. Section 2 provides a brief review of the E86 hurricane model, with the details relegated to an appendix. Section 3 reviews a more complete model for the boundary layer, based on the work of Smith (2003) and Smith and Vogl (2008; henceforth SV08), and examines the approximations made by Emanuel in terms of this model. Solutions of the more complete boundary-layer model with Emanuel's gradient wind profile at the top of the layer are presented and discussed in Section 4. Shown also in this section is the dependence of the boundary-layer flow on the depth

*Correspondence to: Roger K. Smith, Meteorological Institute, University of Munich, Theresienstr. 37, 80333 Munich, Germany.
E-mail: roger.smith@lmu.de*

of the layer and on the breadth of the gradient wind profile at its top. Section 5 discusses some implications of the calculations and Section 6 presents the conclusions.

2. The E86 model in brief

In the E86 model, the hurricane vortex is assumed to be steady and circularly symmetric about its axis of rotation. The boundary layer is taken to have uniform depth, h, and is divided into three regions as shown in Figure 1. Regions I and II encompass the eye and eyewall, respectively, while Region III refers to that beyond the radius, r_m, of maximum tangential wind speed, v_m, at the top of the boundary layer. (Contrary to Emanuel's assumption in this figure, observations show that r_m is located well inside the outer edge of the eyewall, e.g. Figure 3 of Marks *et al.* 2008. The significance of this discrepancy will become clearer in section 5). E86 takes the outer radius of Region II to be r_m on the basis that precipitation-driven downdrafts may be important outside this radius. The tangential wind field above the boundary layer is assumed to be in thermal wind balance and air parcels flowing upwards and outwards into the upper troposphere are assumed to conserve their absolute angular momentum, M, and saturation moist entropy, s^* (calculated reversibly). These surfaces are assumed to flare out in the upper troposphere. Here, s^* is defined by:

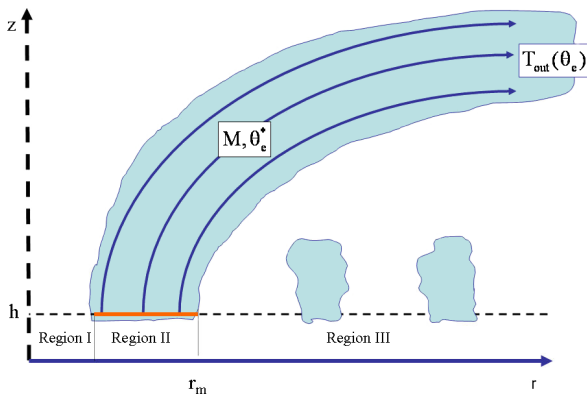$$s^* = c_p \ln \theta_e^*, \qquad (1)$$

Figure 1. Schematic diagram of Emanuel's 1986 model for a mature hurricane. The boundary layer is assumed to have constant depth h and is divided into three regions as shown: the eye (Region I), the eyewall (Region II) and outside the eyewall (Region III) where spiral rainbands and shallow convection emanate into the vortex above. The absolute angular momentum per unit mass, M, and equivalent potential temperature, θ_e, of an air parcel are conserved after the parcel leaves the boundary layer and ascends in the eyewall cloud. The precise values of these quantities depend on the radius at which the parcel exits the boundary layer. The model assumes that the radius of maximum tangential wind speed, r_m, is located at the outer edge of the eyewall cloud, whereas recent observations (e.g. Figure 3 of Marks *et al.*, 2008) indicate that it is closer to the inner edge. This figure is available in colour online at www.interscience.wiley.com/qj

where θ_e^* is the reversible saturation equivalent potential temperature and c_p denotes the specific heat at constant pressure of dry air. Because the saturation vapour pressure of moist air is a unique function of temperature both s^* and θ_e^* are state variables. E86 then integrates the thermal wind equation upwards along these surfaces from radius r to some large radius r_{out} ($>> r$) to obtain a relationship between the radial rates of change of M and s^* at the top of the boundary layer, $z = h$ (see Equation (A12) in the Appendix). This equation may be further integrated with respect to radius to obtain a relationship between θ_e^* and the logarithm of the Exner function at the top of the boundary layer, assuming gradient wind balance prevails at this height:

$$\frac{T_B - \overline{T}_{out}}{T_B} \ln \left(\frac{\theta_e^*}{\theta_{eo}^*} \right) = \ln \left(\frac{\pi_o}{\pi} \right) - \frac{1}{2} \left(r \frac{\partial \ln \pi}{\partial r} \right)$$
$$+ \frac{1}{4} \frac{f^2}{c_p T_B} (r_o^2 - r^2) \quad \text{at } z = h, \qquad (2)$$

where T_B is the temperature at $z = h$, T_{out} is the temperature on the s^* surface at r_{out} and $\overline{T}_{out}$ is an average of this temperature weighted with the saturation moist entropy of the outflow angular momentum surfaces (Equation (A16)), π is the Exner function, f is the Coriolis parameter and the subscript $_o$ denotes a value at some large radius $r = r_o$. So as not to distract from the main presentation, the details are given in the appendix.

The flow in Regions I and II is fully determined by a simple slab formulation for the boundary layer from which a second functional relationship is obtained between M and s^* (Equation (A17)). The two relationships, Equations (A12) and (A17), lead *inter alia* to an expression for the tangential wind speed, V, at $z = h$ in Region II. In this region the Rossby number is large compared to unity and the Coriolis term may be neglected, giving

$$\mu V^2 = \frac{C_k}{C_D} c_p (T_B - T_{out})(\ln \theta_{es}^* - \ln \theta_e^*), \quad \text{at } z = h, \quad (3)$$

where θ_{es}^* is the saturation equivalent potential temperature at the sea surface temperature, C_k and C_D are sea surface exchange coefficients for enthalpy and momentum, and $\mu = V_s/V$, where V_s is the magnitude of the near-surface wind. Equation (3) states that in Region II, V is determined locally by the thermodynamic disequilibrium between the air in the boundary layer and the sea surface and the temperature difference between the top of the boundary layer and the outflow temperature.

E86's boundary-layer formulation in Regions I and II expresses a balance between radial advection and surface gain or loss of azimuthal momentum and specific entropy. In the derivation of Equation (3), the radial velocity is eliminated so that the formula for V^2 is not explicitly dependent on the radial component of velocity in the boundary layer.

Equations (2) and (3) lead essentially to an expression for the pressure as a function of radius (actually the

logarithm of the Exner function) at the top of the boundary layer in Regions I and II (Equations (41) and (45) of E86). On the basis that precipitation-driven downdraughts tend to offset the moistening of inflowing air parcels in Region III, Emanuel assumes that the relative humidity at the top of the surface layer has a constant value of 80% all the way inwards to r_m, an assumption that is not borne out by observations (e.g. Figure 4d of Montgomery *et al.*, 2006). This assumption leads to a second equation relating the equivalent potential temperature to the logarithm of the Exner function and the relative humidity at the top of the surface layer (Equation (A20)). This equation, when combined with Equation (2), gives an expression for the logarithm of the Exner function at $z = h$ in Region III (Equation (39) of E86). With the assumption of gradient wind balance at $z = h$, the resulting two equations for pressure and θ_e^* at this level completely determine the tangential wind speed at the top of the boundary layer at all radii.

Note that the tangential wind speed at the top of Region III is obtained only from thermodynamic considerations in the boundary layer; the dynamics of the boundary layer are completely ignored. It will be argued below that the tacit assumption of gradient wind balance in the boundary layer in Regions I and II and the neglect of boundary-layer dynamics in Region III represent a fundamental limitation of Emanuel's theory and leads to an inconsistency with important ramifications.

3. The boundary layer

To put E86's assumptions regarding the boundary layer in perspective, we review first the simple, but more complete model of the boundary layer of a steady axisymmetric hurricane-like vortex on an f-plane developed by Smith (2003) and SV08. We examine then the consequences of assuming gradient wind balance in the layer.

3.1. A slab model for the boundary layer

The boundary layer in SV08 is assumed again to have uniform depth, h, and constant density. (SV08 considered also the variable depth case, but for simplicity the focus here is on the constant-depth boundary layer assumed by E86.) In a cylindrical coordinate system (r, ϕ, z), the vertically integrated equations expressing the local budgets of radial momentum, azimuthal momentum, heat or moisture, and mass continuity can be written in the following form:

$$u_b \frac{du_b}{dr} = \frac{w_{h_-} + w_{sc}}{h} u_b - \frac{(v_{gr}^2 - v_b^2)}{r}$$
$$- f(v_{gr} - v_b) - \frac{C_D}{h}(u_b^2 + v_b^2)^{\frac{1}{2}} u_b, \quad (4)$$

$$u_b \frac{dv_b}{dr} = \frac{w_{h_-} + w_{sc}}{h}(v_b - v_{gr}) - (\frac{v_b}{r} + f)u_b$$
$$- \frac{C_D}{h}(u_b^2 + v_b^2)^{\frac{1}{2}} v_b, \quad (5)$$

$$u_b \frac{d\chi_b}{dr} = \frac{w_{h_-} + w_{sc}}{h}(\chi_b - \chi_{h+})$$
$$+ \frac{C_\chi}{h}(u_b^2 + v_b^2)^{\frac{1}{2}}(\chi_s - \chi_b) - \dot{\chi}_b, \quad (6)$$

$$\frac{du_b}{dr} = -\frac{u_b}{r} - \frac{w_h}{h}, \quad (7)$$

where u_b and v_b are the radial and azimuthal components of velocity in the boundary layer, $v_{gr}(r)$ and w_h are the tangential velocity and vertical velocity at the top of the boundary layer, $w_{h_-} = \frac{1}{2}(w_h - |w_h|)$, χ_b is a scalar quantity, which could be the dry static energy, the specific humidity, or the specific entropy, f is the Coriolis parameter, C_D is the surface drag coefficient, C_χ is the surface transfer coefficient for χ_b, χ_{h+} is the value of χ just above the boundary layer, and χ_s is the value of χ at the sea surface. The terms involving w_{sc} represent turbulent fluxes at the top of the boundary layer (arising from rainbands, shallow convection, or smaller-scale turbulent structures) and the term $\dot{\chi}_b$ represents the effects of radiative cooling and dissipative heating when χ_b is taken to be the dry static energy or specific entropy. Consistent with the slab boundary-layer formulation, the quantities u_b, v_b and χ_b are assumed to be independent of depth. Note that w_{h_-} is nonzero only when $w_h < 0$, in which case it is equal to w_h. Thus the terms involving w_{h_-} represent the transport of properties from above the boundary layer that may be different from those inside the boundary layer. For the calculations presented in sections 4.1 and 4.2 we take C_D to be a constant, equal to 2.0×10^{-3}, the value use by E86. For those in section 4.3, we follow SV08 and take $C_D = C_{D0} + C_{D1}|\mathbf{u}_b|$, where $C_{D0} = 0.7 \times 10^{-3}$ and $C_{D1} = 6.5 \times 10^{-5}$ for wind speeds less than 20 m s^{-1} and $C_D = 2.0 \times 10^{-3}$, a constant, for larger wind speeds. These values are based on our interpretation of Figure 5 from Black *et al.* (2007). In the calculations described in section 4, we consider only dynamical effects, so that a value for C_χ is not required.

Substitution of Equation (7) into (4) gives an expression for w_h:

$$w_h = \frac{h}{1+\alpha} \left[\frac{1}{u_b} \left\{ \frac{v_{gr}^2 - v_b^2}{r} + f(v_{gr} - v_b) \right. \right.$$
$$\left. \left. + \frac{C_D}{h}(u_b^2 + v_b^2)^{\frac{1}{2}} u_b \right\} - \frac{u_b}{r} \right], \quad (8)$$

where α is zero if the expression in square brackets is positive and unity if it is negative. With this expression for w_h, Equations (4)–(6) together with (8) form a system of ordinary differential equations that may be integrated radially inwards from some large radius R to find u_b, v_b and χ_b as functions of r, given values of these quantities at $r = R$ as well as the radial profile $v_{gr}(r)$.

3.2. E86's approximations for the boundary layer

Emanuel writes Equation (5) in terms of the absolute angular momentum in the boundary layer, $M_b = rv_b +$

$fr^2/2$, and approximates this equation in Region II, where $w_h > 0$, as

$$u_b \frac{dM_b}{dr} = -\frac{C_D}{h} r v_b^2. \tag{9}$$

Here it is assumed that $w_{sc} = 0$ and that $u_b^2 << v_b^2$ in the drag term. Note that, in general, *knowledge of u_b is required for the determination of M_b*. However, Emanuel does not use the radial momentum equation to determine u_b, as his main focus is to obtain an expression relating the specific entropy, s_b, to M_b (Equation (A17)). (In fact, E86 uses Equation (9) to determine u_b, having obtained the radial pressure distribution through his Equations (39) and (41) and having tacitly assumed gradient wind balance to obtain v_b.) In the region where $w_h > 0$, the equation for the specific entropy is

$$u_b \frac{ds_b}{dr} = \frac{C_k}{h} v_b (s_s^* - s_b), \tag{10}$$

where s_s^* is the saturation specific humidity at the sea surface and again it is assumed that $w_{sc} = 0$ and the total wind speed has been approximated by the tangential wind speed.

E86's assumption that air leaving the boundary layer conserves its absolute angular momentum implies that $v_{gr} = v_b$ where $w_h > 0$. The assumption also that v_{gr} is in gradient wind balance implies that v_b is in gradient wind balance. This is a rather strong assumption for the boundary layer in the inner core of a rapidly rotating vortex and although it has been made by previous authors (e.g. Ooyama, 1969), we are not aware of any rigorous justification for it. In fact it is not supported by a scale analysis of the boundary-layer equations (e.g. Smith, 1968). Ooyama was certainly aware of the limitations of the assumption and wrote in an unpublished manuscript in 1968:

> ... *it appears that the weakest hypothesis in [his] original model is the use of the balance approximation in the boundary layer.*

In this manuscript, Ooyama went on to show that the solutions in a calculation with a more complete boundary-layer formulation were more realistic than those with a balanced boundary-layer formulation. Indeed it is precisely the lack of gradient wind balance in the boundary layer that gives rise to the 'frictionally driven' inflow in the layer.

While inflow is theoretically possible in a boundary layer that is in approximate gradient wind balance, the balance assumption can be justified only if the radial acceleration and radial friction terms are small compared with the radial pressure gradient and the sum of the centrifugal and Coriolis forces. In such a 'balanced' formulation, the radial flow is determined by the (*sic*) tangential momentum equation. With Emanuel's assumption that the total wind speed in the friction term

in Equation (5) can be reasonably approximated by v_{gr}, the equation predicts that

$$u_b = -c v_{gr}, \tag{11}$$

where $c = C_d v_{gr}/(h \zeta_a)$, and $\zeta_a (= \zeta + f)$ and ζ are the absolute vorticity and relative vorticity of the gradient wind, v_{gr}, respectively. Other processes could contribute also to radial motion in a boundary layer that is closely in gradient wind balance. One example is a radial buoyancy gradient above the boundary layer associated with moist convective processes (e.g. Smith, 2000; Smith *et al.*, 2005).

In the next section we examine solutions of the dynamical component of the full boundary-layer equations (4), (5) and (7) with the gradient wind speed v_{gr} obtained by E86. We show that these solutions are incompatible with the assumption in the E86 model that $v_{gr} = v_b$ where $w_h > 0$. We show further that the lack of any dynamical constraint in the boundary layer in Region III other than the tacit assumption of gradient wind balance is another major deficiency of the theory.

4. Calculations

4.1. The E86 gradient wind profile

Figure 2 shows calculations of the full boundary-layer equations of Section 3.1, taking the gradient wind speed profile $v_{gr}(r)$ and other parameters the same as those obtained by E86. In particular $f = 6.83 \times 10^{-5}$ s^{-1}, corresponding with a latitude of 28 °N, $h = 1000$ m, $C_D = 2.0 \times 10^{-3}$, $T_s = 27$ °C, $T_B = 27$ °C and $\overline{T}_{out} = -67$ °C. The radial profile of v_{gr} is obtained by solving the gradient wind equation with the pressure profile derived from the pair of expressions relating $\ln \pi$ and θ_e^* in E86, namely Equations (39) and (41), using the parameter values detailed in that paper. The integration in the full boundary-layer calculation starts at a radius of 375 km, where the gradient wind speed (only 1.73 m s^{-1}) is small enough to justify the neglect of the nonlinear acceleration terms in the equations (section 4 of Smith, 2003). (Note that beyond a radius of 400 km, the tangential wind in Emanuel's calculation is anticyclonic and just inside this radius, at about 396 km, the profile is inertially unstable.) Figure 2(a) compares the full solution for the tangential wind speed in the boundary layer, v_b, with the imposed gradient wind speed v_{gr}. It compares also the full solution for the radial wind speed, u_b, with that obtained from Equation (11) based on the balance assumption that $v_{gr} = v_b$ as made by E86, and assuming that $w_{sc} = 0$. We designate the balanced solution for u_b as u_E and that for the corresponding vertical motion at the top of the boundary layer as w_E. We calculate the latter from the continuity equation (7) using centred differences. The profiles of vertical velocity at the top of the boundary layer in the full solution, w_h, is compared with that in the balanced solution in Figure 2(b). It is worth noting at
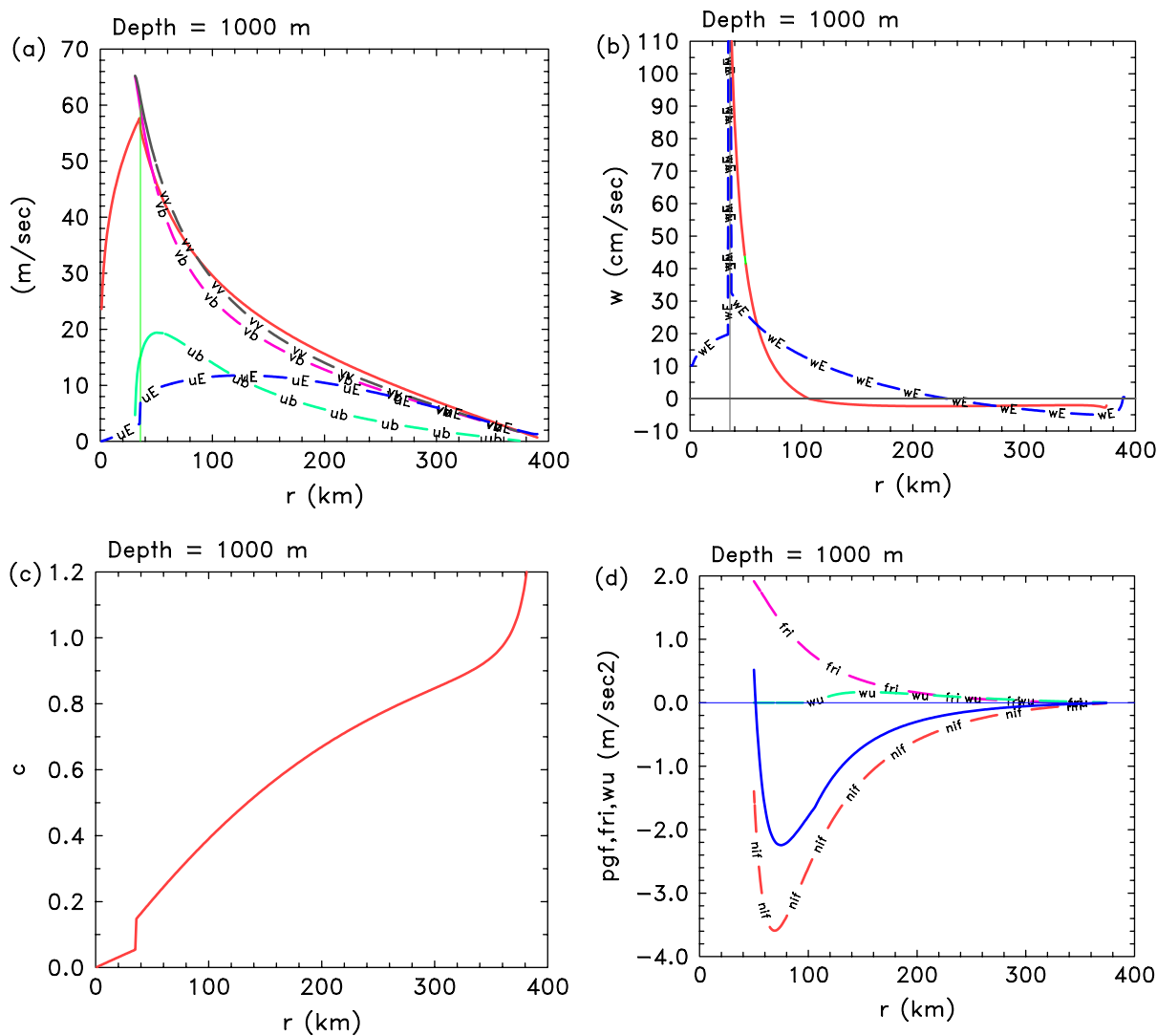
Figure 2. (a) Radial profiles of boundary-layer radial (u_b) and tangential (v_b) wind components and the total wind speed $\sqrt{(u_b^2 + v_b^2)}$ (denoted vv) from the full boundary-layer solution, and the tangential wind speed above the boundary layer (v_{gr}) as obtained by E86 (solid curve). Also shown is the radial flow obtained from the balanced solution determined from Equation (11) and denoted by u_E. Units are m s^{-1}. For plotting convenience, the signs of u_b and u_E have been reversed. The profile of v_{gr} is indicated by the unmarked solid curve. (b) Corresponding radial profiles of vertical velocity at the top of the boundary layer (w_h) and that in the balanced solution (w_E). Units are cm s^{-1}. The thin vertical line in (a) and (b) marks the radius of maximum v_{gr}, the boundary between Regions II and III in Figure 1. (c) Radial profile of the coefficient c in Equation (11). (d) Radial profiles of the three terms on the right-hand side of the radial momentum equation, Equation (4), and their sum (the solid line) for the full solution. The designation 'wu', 'nif' and 'fri' refer to the first, second and third terms in the equation, representing the downward advection of radial momentum, the net inward force and the frictional force, respectively. This figure is available in colour online at www.interscience.wiley.com/qj

this point that this balanced solution agrees closely with that shown by E86 in his Figure 12.

In the full and balanced calculations, the radial wind component increases inwards to a certain radius and then decreases. However, there are significant quantitative differences in the profiles. In the balanced solution, the maximum inflow of about 12 m s^{-1} occurs at a comparatively large radius (130 km), while in the full solution it occurs at 52 km, a little outside the radius of maximum gradient wind speed (35.8 km). These differences occur despite the fact that beyond 100 km in radius, v_b is at most 18% smaller than v_{gr}, showing that the degree of gradient wind imbalance is important. The decline in u_E from such a large radius is a result of the decline in the

parameter c with decreasing radius (Figure 2(c)), which is larger than the rate at which v_{gr} increases. The discontinuity in u_E at $r = r_m$ is a result of the discontinuity of the relative vorticity ζ at this radius, which leads to a discontinuity in c. As expected there are correspondingly large differences in the profiles of vertical velocity at the top of the boundary layer (Figure 2(b)). In particular, the change from descent at large radii to ascent at small radii occurs at a much smaller radius in the full calculation: 107 km compared with 230 km.

Of particular significance is the difference between v_b and v_{gr} in the inner core region, near the radius of maximum gradient wind speed. Here the tangential wind in the boundary layer becomes supergradient (i.e. v_b exceeds

v_{gr}), which is incompatible with Emanuel's assumption that v_{gr} is equal to v_b at radii where $w_h > 0$. In other words, *Emanuel's calculated PI (i.e. v_m) is exceeded when a more complete boundary layer formulation is used*. The occurrence of supergradient winds is a reflection of the strong radial inflow which advects absolute angular momentum at a rate larger than it can be removed locally by the frictional torque (SV08). As soon as the tangential wind speed becomes supergradient, all forces in the radial momentum equation act outwards and lead to a rapid deceleration of the inflow. In the full boundary-layer solution, the radial flow becomes zero at some finite radius and the boundary-layer model becomes singular at this radius. In reality we would expect the inflow to be expelled upwards before this radius, carrying its horizontal momentum with it. If the upflow remains out of balance, we would expect it to flow outwards immediately above the inflow layer, a behaviour which is shown by full numerical solutions (e.g. Figures 3c, 6c of Montgomery *et al.*, 2001; Figure 1b of Persing and Montgomery, 2003).

Figure 2(d) shows the radial variation of the force terms in the radial momentum equation, Equation (4). The term representing the downward transport of radial momentum, that proportional to w_{h-}, is non-zero only in the outer region and is small compared with the other terms. At larger radii, the net *inward* force (the difference between the inward pressure gradient and outward centrifugal and Coriolis forces) is larger in magnitude than the outward frictional force. Moreover, the inward radial acceleration, which is equal to the net *total* radially inward force, is particularly large at radii less than 150 km.

4.2. Dependence on boundary-layer depth

The boundary-layer constraint in Emanuel's theory is independent of the assumed boundary-layer depth. (Note that the depth cancels in applying E86's boundary-layer

Figure 3. As Figure 2(a), but for a boundary layer depth of 600 m. This figure is available in colour online at www.interscience.wiley.com/qj

formulation to derive Equation (A17) in the appendix.) However, this depth has a significant influence on the full boundary-layer solution because the effective drag in the boundary layer is inversely proportional to the depth (SV08). For this reason we repeated the foregoing boundary-layer calculations for a boundary-layer depth of 600 m. These calculations are shown in Figure 3. The increased effective friction leads to a larger reduction of the tangential wind speed in the boundary layer than in the earlier calculation and therefore to a larger net inward force and a larger inward acceleration. Consequently the maximum inflow is considerably larger than before (36 m s^{-1} instead of 19 m s^{-1}) and occurs at a smaller radius (32 km instead of 52 km). On the other hand, the balanced solution changes only in magnitude and not in shape, whereupon the maximum occurs at 130 km as before. This result follows directly from Equation (11) because the decreased depth simply increases the coefficient c by a constant factor at all radii and the gradient wind profile is the same. The fact that the maximum tangential wind speed in the boundary layer in this calculation is considerably higher than in the previous one implies that the PI of the steady vortex is sensitive to the boundary-layer depth, an important point not emphasized in E86 and his subsequent papers. (Whereas the E86 model and the more complete boundary-layer model furnish non-negligible, but modest differences in the maximum tangential wind ($\sim$10–20%), it should be remembered that the boundary-layer model used here precludes any thermodynamic and dynamic feedbacks between the boundary layer and interior flow. For several reasons, this feedback is thought to be quantitatively significant; see section 5).

4.3. Dependence on vortex size

Given the importance of the radial acceleration in the boundary layer as demonstrated above, the inclusion of boundary-layer dynamics in Region III of Emanuel's model may be expected to have important consequences for the tangential wind maximum also. We illustrate these consequences by a third set of calculations to emphasize the dependence of the maximum boundary-layer wind speed on the vortex size. These calculations are based on solutions of the full boundary-layer equations with the different profiles of gradient wind speed shown in Figure 4. These profiles are defined in Smith (2003) and are inertially stable for the value of f used earlier. The solutions for these profiles are shown in Figure 5 for a boundary-layer depth of 800 m, a radially varying drag coefficient C_D as discussed in Section 3.1, and with $w_{sc} = -5.7$ cm s^{-1}, the value used in SV08. Note that there is a clear dependence of the solution on storm size, as might be characterized, for example, by the radius of gale-force winds (17 m s^{-1}) above the boundary layer. As the storm size decreases, the radius of maximum inflow decreases and the maximum inflow increases. Moreover, the radius at which the vertical
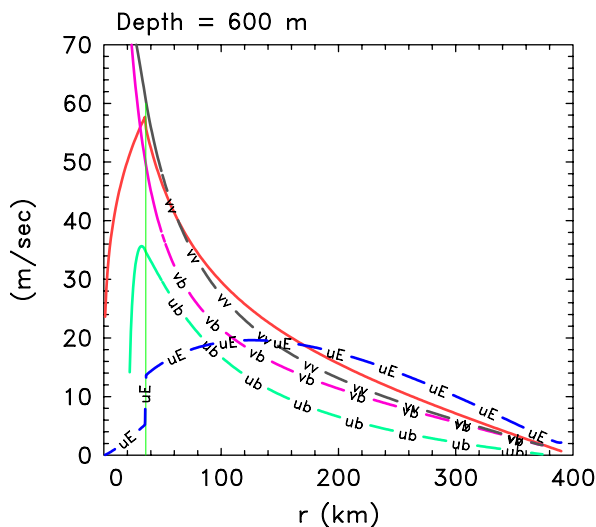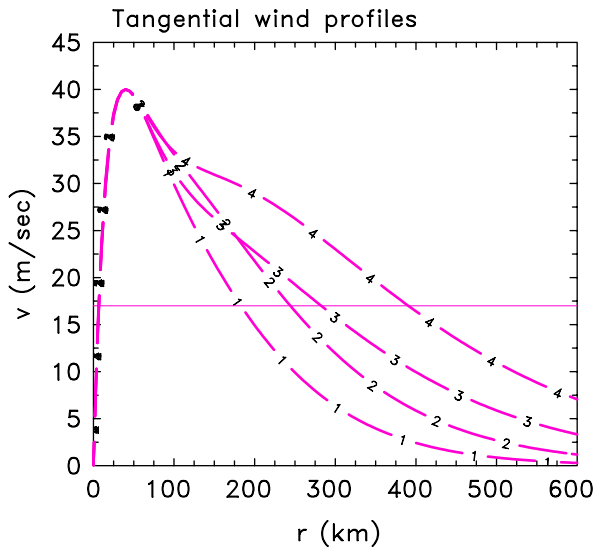
Figure 4. Four radial profiles of tangential wind speed, $v_{gr}(r)$, at the top of the boundary layer used for the calculations shown in Figure 5. The thin horizontal line indicates the radius of gale force winds (17 m s^{-1}). This figure is available in colour online at www.interscience.wiley.com/qj

velocity changes sign decreases (figure not shown). To the extent that the intensity is controlled by boundary-layer dynamics, these solutions show a clear dependence on the size of the outer circulation, so that the PI of midget storms may be expected to be different from that of broad storms. These solutions highlight the dependence of the flow at all radii in the boundary layer on the size of the vortex above.

5. Discussion

Using the gradient wind profile predicted by Emanuel's steady-state hurricane model in conjunction with a more complete formulation of the boundary layer generally

leads to the occurrence of supergradient winds in the boundary layer in the high wind region of the vortex. These are incompatible with a key assumption in Emanuel's derivation of the gradient wind profile that requires it to be equal to that in the boundary layer where the flow is upwards out of the boundary layer. Moreover, the degree to which the boundary-layer winds are supergradient increases as the boundary-layer depth decreases. In reality, the vertical advection of the supergradient winds out of the boundary layer would lead to outflow until a radius is achieved at which the pressure gradient is matched to that which can be sustained by the mass distribution. Of course, this effect cannot be captured by a one-layer model, but it is significant that calculations in which the boundary layer is allowed to adjust to an outer flow do show such behaviour (e.g. Figures 3c, 6c of Montgomery *et al.*, 2001; Figure 1b of Persing and Montgomery, 2003).

The dependence of the radius at which subsidence at large radii changes to ascent, r_{up}, as well as the predicted radial profiles of u_b, v_b and w_h, on the tangential wind profile above the boundary layer where there is subsidence into it shows that the dynamics of the boundary layer in Region III of Figure 1 cannot be ignored.

The foregoing considerations suggest an alternative subdivision of the boundary layer to that in Figure 1. This alternative is sketched in Figure 6 and is based on whether the top of the boundary layer is an inflow boundary (Region B, $r > r_{up}$) or an outflow boundary (Region A, $r < r_{up}$). In Region B, the boundary layer is directly influenced by the vortex above through the radial pressure gradient at the top of the layer and through the downward advection of free vortex properties such as moisture, heat and momentum. Except possibly through the occurrence of moist convection, there is no essential feedback to the free vortex. (An important exception arises with the occurrence of spiral rainbands and
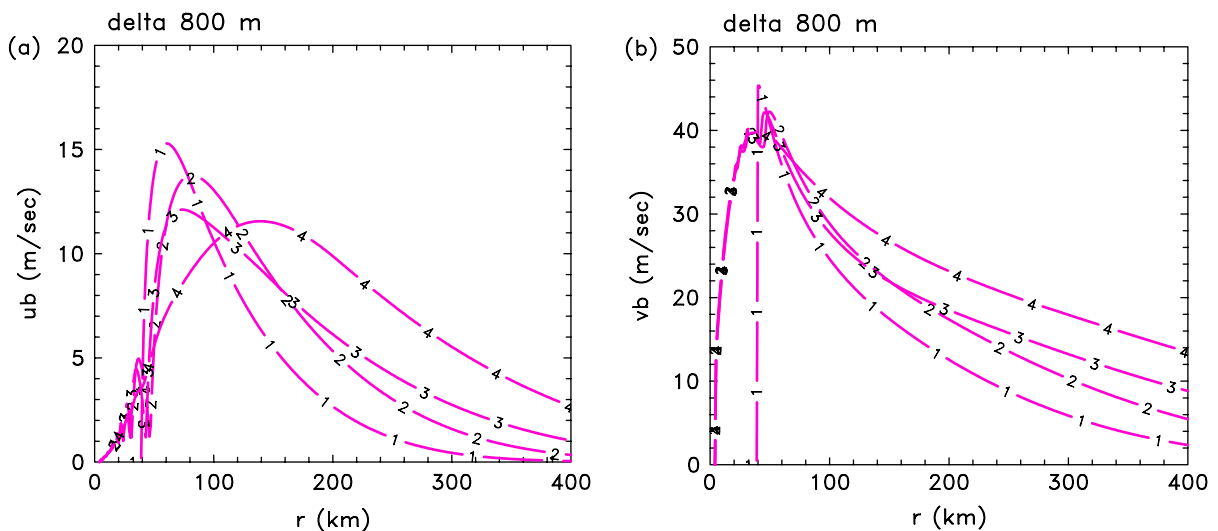

Figure 5. Radial profiles of (a) the *radially inward* and (b) the tangential components of wind speed in the boundary layer for the four vortex profiles shown in Figure 4. This figure is available in colour online at www.interscience.wiley.com/qj
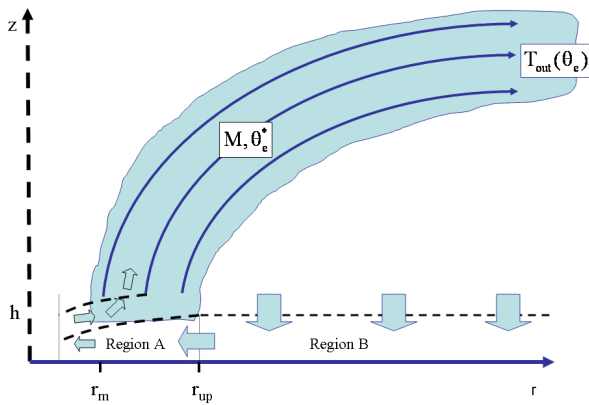
Figure 6. Modified conceptual model of the hurricane inner-core region motivated by the findings herein together with recent observational and modelling studies. Air subsides into the boundary layer for $r > r_{up}$ and ascends out of the boundary layer for $r < r_{up}$. The frictionally induced net inward force in the outer region produces a radially inward jet at $r = r_{up}$. The subsequent evolution of this jet depends on the bulk radial pressure gradient that can be sustained by the mass distribution at the top of the boundary layer. The jet eventually generates supergradient tangential winds whereafter the radial flow rapidly decelerates and turns upwards and outwards. When the outflow has adjusted to the radial pressure gradient that is sustained by the mass field, the flow turns upwards into the eyewall clouds. See sections 5 and 6 for further details. This figure is available in colour online at www.interscience.wiley.com/qj

the corresponding formation of one or more secondary eyewalls (Houze *et al.*, 2007; Terwey and Montgomery, 2008). These asymmetric processes, their coupling to the boundary layer and the free axisymmetric vortex are not yet well understood and consequently lie beyond the scope of the present model.) However, in Region A, boundary-layer properties are advected into the free vortex and have a profound influence on its structure. We may think of the boundary-layer flow in Region B as producing an inward radial jet at $r = r_{up}$, the strength of which depends on the gradient wind profile at larger radii as well as on the boundary-layer depth. The boundary-layer dynamics in Region A determine the fate of this jet, but the details depend *inter alia* on the radial pressure gradient at the top of the boundary layer, i.e. there is a substantial two-way feedback between the boundary layer and the free vortex in this region. These details depend also on the boundary-layer depth. The radial pressure gradient in the boundary layer is probably still determined in large measure by the mass distribution in the free vortex, with possible exceptions in localized regions near where inflow turns to upflow and possibly outflow (see below). However the free vortex can be expected to be strongly influenced by the radial distribution of mass, momentum and moisture that leave the boundary layer.

The calculations presented here, supported by those of SV08, show that the tangential winds tend to become supergradient in the inner core and, as a result, the radial flow rapidly decelerates until the tangential component becomes subgradient again, or the radial wind becomes zero (a point at which the boundary-layer equations in a one-layer model become singular and a more

sophisticated technique beyond the scope of this study is required for matching the solutions inside and outside this radius). In either case, the flow out of the boundary layer increases markedly. If the winds carried upwards retain their supergradient character they will surely flow with a significant component outwards until they have come into gradient wind adjustment with the mass field aloft. At this point they would be expected to turn upwards into the eyewall. While parts of this scenario are speculative at this stage, the foregoing ideas would explain the observations of a skirt of moderate to high radar reflectivity adjacent to the main eyewall (e.g. Figures 5–7 of Aberson *et al.*, 2006; Figure 3 of Marks *et al.*, 2008), but still within the 'visible' eye defined by the upper-tropospheric boundary of clear and cloudy air seen in high-resolution satellite imagery (e.g. Figure 2 of Bell and Montgomery, 2008) and they are consistent with the calculations of Montgomery *et al.* (2001, Figures 3c, 6c) and Persing and Montgomery (2003, Figure 1b).

Within the context of the axisymmetric model, the thermodynamic consequences of the overshoot/adjustment region have been demonstrated to be non-trivial as moist air near the surface and within the maximum tangential wind (including the outer part of the 'eye') can be drawn into the main eyewall above the shallow inflow layer. This low-level air generally possesses higher equivalent potential temperature than air found at the radius of maximum wind due to a lower surface pressure and non-zero surface winds and contributes additional heat and local buoyancy to the eyewall (Persing and Montgomery, 2003; Cram *et al.*, 2007). The net result is an enhancement of the radial gradient of equivalent potential temperature above the inflow layer that supports strong tangential winds in accordance with axisymmetric thermal wind balance above the boundary layer (Appendix in Montgomery *et al.*, 2006). In light of these findings, together with the recognition that shear instability and coherent vortex substructures bordering the eye and eyewall will contribute to the aforementioned adjustment process (Schubert *et al.*, 1999; Montgomery *et al.*, 2002; Braun *et al.*, 2006), we believe that both the initial vortex structure and interactions between the eye and eyewall region are important elements of intense storms and should be accounted for in hurricane intensity theory.

Note that much of the foregoing discussion was based on the assumption that the main dynamical processes in tropical cyclones are axisymmetric. However, recent calculations by Nguyen *et al.* (2008) have highlighted the importance of asymmetric processes in the intensification of these storms. A comprehensive synthesis of these findings with the insights obtained here is a goal for future work.

6. Conclusions

We have shown that the tacit assumption of gradient wind balance in the boundary layer is a major deficiency of Emanuel's steady-state hurricane model and also,

by implication, his theory for the potential intensity of hurricanes. Although the vertically integrated tangential wind in the boundary layer is usually no more than 15–20% less than its gradient wind counterpart, a fact that makes gradient wind balance a seemingly defensible zero-order approximation locally, we have shown that the global consequences of this simplification on the inner-core structure of intense storms are non-trivial. Indeed, the boundary layer owes its existence to gradient wind imbalance that results from a reduction of the tangential wind speed by friction. When such imbalance is allowed for by the inclusion of a non-trivial radial momentum equation in the theory, the boundary-layer flow depends on the tangential wind structure above the boundary layer, a feature that must be taken into account in an improved theory for hurricane PI.

We conclude that it is not permissible to make the gradient balance assumption in the inner region and that, in a realistic model of a hurricane, the radial pressure gradient above the boundary layer must be prescribed or determined independently of the boundary layer. Nevertheless, even in this case, the solutions show a mismatch between the predicted mean winds in the boundary layer and those prescribed above where the flow is out of the layer. This mismatch suggests that the outflow jet found above the inflow layer in full numerical solutions for the boundary layer, together with the flow above it, is a means by which the flow exiting the boundary layer adjusts to the radial pressure gradient associated with the vortex above the boundary layer. The implication would be that a more complete formulation of the (steady) boundary layer in the inner core region of a tropical cyclone using a slab-type formulation would require at least two layers including one to represent the outflow jet. This layer is required to allow the radial and tangential wind fields to adjust to the radial pressure gradient implied by the mass distribution in the free troposphere. Such a formulation would appear to be a necessary component of a more consistent and accurate theory for hurricane PI and such a theory must take into account the vortex size and the boundary-layer depth.

Appendix

Derivation of Equation (3)

In pressure coordinates, the gradient wind equation and hydrostatic equation may be written as:

$$g \left(\frac{\partial z}{\partial r} \right)_p = \frac{M^2}{r^3} - \tfrac{1}{4} r f^2, \tag{A1}$$

and

$$g \left(\frac{\partial z}{\partial p} \right)_r = -\alpha, \tag{A2}$$

where α is the specific volume, p is the pressure, z is the height of a pressure surface and g is the acceleration due to gravity. Eliminating the geopotential height of the pressure surface, gz, gives an alternative form of the thermal wind equation:

$$\frac{1}{r^3} \left(\frac{\partial M^2}{\partial p} \right)_r = - \left(\frac{\partial \alpha}{\partial r} \right)_p. \tag{A3}$$

Since s^* is a state variable, α can be regarded as a function of p and s^*. Then with a little manipulation (14) becomes the thermal wind equation:

$$\frac{1}{r^3} \left(\frac{\partial M^2}{\partial p} \right)_r = - \left(\frac{\partial \alpha}{\partial s*} \right)_p \left(\frac{\partial s^*}{\partial r} \right)_p. \tag{A4}$$

E86 invokes one of the Maxwell relations for moist saturated air in the form

$$\left(\frac{\partial \alpha}{\partial s^*} \right)_p = \left(\frac{\partial T}{\partial p} \right)_{s*}, \tag{A5}$$

so that (15) becomes

$$\frac{1}{r^3} \left(\frac{\partial M^2}{\partial p} \right)_r = - \left(\frac{\partial T}{\partial p} \right)_{s*} \left(\frac{\partial s^*}{\partial r} \right)_p. \tag{A6}$$

With the assumption that M and s^* surfaces coincide, i.e. $M = M(s^*)$, (17) becomes

$$\frac{2M}{r^3} \left(\frac{\partial M}{\partial p} \right)_r = - \left(\frac{\partial T}{\partial p} \right)_{s*} \frac{\mathrm{d}s^*}{\mathrm{d}M} \left(\frac{\partial M}{\partial r} \right)_p. \tag{A7}$$

Note that $(\partial T / \partial p)_{s*}$ is just the temperature lapse rate as a function of pressure along a moist adiabat. Now along an M surface,

$$\left(\frac{\partial M}{\partial r} \right)_p \mathrm{d}r + \left(\frac{\partial M}{\partial p} \right)_r \mathrm{d}p = 0, \tag{A8}$$

so that the slope of an M surface in (r, p) space is

$$\left(\frac{\mathrm{d}r}{\mathrm{d}p} \right)_M = - \left(\frac{\partial M}{\partial p} \right)_r \bigg/ \left(\frac{\partial M}{\partial r} \right)_p. \tag{A9}$$

Combining (A7) and (A9), the thermal wind equation (A6) becomes

$$\frac{1}{2}\left(\frac{\mathrm{d}r^{-2}}{\mathrm{d}p}\right)_M = -\frac{1}{2M}\left(\frac{\partial T}{\partial p}\right)_{s*}\frac{\mathrm{d}s^*}{\mathrm{d}M}, \tag{A10}$$

which may be integrated upwards along the M (or s^*) surface starting from the top of the boundary layer $z = h$ to an outer radius r_{out} to give

$$\frac{1}{r^2}\bigg|_M - \frac{1}{r_{out}^2}\bigg|_M = -\frac{1}{M}\frac{\mathrm{d}s^*}{\mathrm{d}M}[T - T_{out}(s^*, p_{out})], \tag{A11}$$

Assuming that $r_{out} \gg r$, and using the chain rule, (A11) gives

$$-[T_B - T_{out}(s^*, p_{out})]\frac{\partial s^*}{\partial r} = \frac{1}{2r^2}\frac{\partial M^2}{\partial r}, \text{ at } z = h, \tag{A12}$$

where T_B is the temperature at the top of the boundary layer and T_{out} is the outflow temperature along the M (or s^*) surface at r_{out}. Using the Exner function, $\pi = (p/p_o)^\kappa$, instead of pressure, the gradient wind equation (A1) takes the form

$$M^2 = r^3\left[c_p T_B\left(\frac{\partial \ln \pi}{\partial r}\right)_z + \frac{1}{4}rf^2\right]. \tag{A13}$$

In the expression for π, $\kappa = R/c_p$, where R is the specific gas constant and p_o is a constant pressure, taken by E86 to be 1015 mb. Substituting (A13) into (A12) results in

$$-\frac{T_B - T_{out}(s^*, p_{out})}{T_B}\frac{\partial \ln \theta_e^*}{\partial r}$$
$$= \frac{\partial \ln \pi}{\partial r} + \frac{1}{2}\frac{\partial}{\partial r}\left(r\frac{\partial \ln \pi}{\partial r}\right) + \frac{1}{2}\frac{rf^2}{c_p T_B}, \text{ at } z = h, \tag{A14}$$

where it is assumed that $\theta_e = \theta_e^*$ at $z = h$. This equation is integrated with respect to radius from r to some large radius $r = r_o$, where it is assumed that $\ln \pi/\pi_o$ and its radial derivative vanish, π_o being the value of π at $z = h$ and $r = r_o$. Remembering that T_B is assumed to be constant, the result is

$$-\ln \theta_{eo}^* + \ln \theta_e^* + \frac{1}{T_B}\int_r^{r_o} T_{out}(s^*, p_{out})\frac{\partial \ln \theta_e}{\partial r}\mathrm{d}r$$
$$= \ln \pi_o - \ln \pi + \frac{1}{2}\left(r\frac{\partial \ln \pi}{\partial r}\right)_o - \frac{1}{2}\left(r\frac{\partial \ln \pi}{\partial r}\right)$$
$$+ \frac{1}{4}\frac{f^2}{c_p T_B}(r_o^2 - r^2), \text{ at } z = h. \tag{A15}$$

Emanuel defines

$$\overline{T}_{out} = \frac{1}{\ln(\theta_e^*/\theta_{eo}^*)}\int_{\ln \theta_{eo}^*}^{\ln \theta_e^*} T_{out}\, \mathrm{d}(\ln \theta_e^*), \tag{A16}$$

which is an average outflow temperature weighted with the saturation moist entropy of the outflow angular momentum surfaces. Remember that θ_e^* along angular momentum surfaces is taken equal to the equivalent potential temperature, θ_e, where the surfaces meet the top of the boundary layer. Then (A15) gives Equation (2).

It is at this point that boundary-layer considerations are invoked. Assuming a slab boundary-layer model with uniform depth as described in section 3.2, E86 derives a further relationship between the specific moist entropy of the boundary layer, s, and M by effectively dividing (10) by (9). We recognize here that the near-surface wind may be different from that at the top of the boundary layer. Thus following E86, but allowing for a reduced surface wind, we obtain

$$\left.\frac{\mathrm{d}s^*}{\mathrm{d}M}\right|_{z=h} = \left.\frac{\tau_s}{\tau_M}\right|_{z=0}, \tag{A17}$$

where $\tau_s = -c_p C_k|\mathbf{V}_s|(\ln \theta_e - \ln \theta_{es}^*)$ and $\tau_M = -C_D|\mathbf{V}_s|rV_s$ are the surface fluxes of enthalpy and momentum expressed by standard aerodynamic formulae, and $|\mathbf{V}_s|$ is the magnitude of the near-surface horizontal velocity. Other quantities are defined in section 2. In the derivation of (A17), it is assumed that the specific entropy, s, and the equivalent potential temperature, θ_e, are uniform across the boundary layer and that the air at the top of the sub-cloud layer is saturated so that $s_b = s^*$ and $\theta_e = \theta_e^*$. This equation can then be blended with (A11) above. (A12) then gives

$$\ln \theta_e^* = \ln \theta_{es}^* - \mu\frac{C_D}{C_k}\frac{1}{c_p(T_B - T_{out})}\left(V^2 + \frac{1}{2}rfV\right),$$
$$\text{at } z = h, \tag{A18}$$

where M has been expressed in terms of the tangential wind speed V at $z = h$. In Region II, $rf \ll V$ so that the second term in parentheses on the right of (A18) can be neglected compared with V^2 and the equation may be written as

$$\mu V^2 = \frac{C_k}{C_D}c_p(T_B - T_{out})(\ln \theta_{es}^* - \ln \theta_e^*), \text{ at } z = h, \tag{A19}$$

where $\mu = V_s/V$. (A19) is (3) in section 3.1 and is a cornerstone of the current EPI-theory (Emanuel, 1995; Bister and Emanuel, 1998).

A further important relationship in Emanuel's theory is that between θ_e^* and the pressure and humidity at the top of the surface layer, which may be written

$$\ln\frac{\theta_e^*}{\theta_{ea}^*} = -\ln\frac{\pi_s}{\pi_a}\left(1 + \frac{Lq_a^* RH_s}{RT_s}\right)$$
$$+ \frac{Lq_a^*}{RT_s}(RH - RH_a)_s \text{ at } z = h, \tag{A20}$$

where L is the latent heat of vaporization, q is the water vapour mixing ratio, RH is the relative humidity, and T is the absolute temperature. The subscript 'a' denotes

the ambient value; as above, a subscript 's' denotes a value at the top of the surface layer and a superscript * denotes a saturation value. This equation is the same as Equation (25) in E86 if one assumes that the reference pressure in the definition of the Exner function is p_a rather than 1000 mb as is usual.

References

Aberson SD, Montgomery MT, Bell MM, Black ML. 2006. Hurricane Isabel (2003): New insights into the physics of intense storms. Part II – Extreme localized wind. *Bull. Am. Meteorol. Soc.* **87**: 1349–1357.

Bell MM, Montgomery MT. 2008. Observed structure, evolution, and potential intensity of category 5 hurricane Isabel (2003) from 12 to 14 September. *Mon. Weather Rev.* in press.

Bengtsson L, Hodges KI, Esch M, Keenlyside N, Komblush L, Luo JJ, Yamagata T. 2007. How may tropical cyclones change in a warmer climate? *Tellus* **59A**: 539–561.

Bister M, Emanuel KA. 1998. Dissipative heating and hurricane intensity. *Meteorol. Atmos. Phys.* **65**: 233–240.

Black PG, D'Asaro EA, Drennan WM, French JR, Niiler PP, Sanford TB, Terrill EJ, Walsh EJ, Zhang JA. 2007. Air-sea exchange in hurricanes: Synthesis of observations from the coupled boundary layer air-sea transfer experiment. *Bull. Am. Meteorol. Soc.* **88**: 357–374.

Braun SA, Montgomery MT, Pu A. 2006. High-resolution simulation of hurricane Bonnie (1998). Part I: The organization of eyewall vertical motion. *J. Atmos. Sci.* NASA/CAMEX special issue, **63**: 19–42.

Camp JP, Montgomery MT. 2001. Hurricane maximum intensity: past and present. *Mon. Weather Rev.* **129**: 1704–1717.

Cram TA, Persing J, Montgomery MT, Braun SA. 2007. A Lagrangian trajectory view on transport and mixing processes between the eye, eyewall, and environment using a high-resolution simulation of hurricane Bonnie (1998). *J. Atmos. Sci.* **64**: 1835–1856.

Emanuel KA. 1986. An air-sea interaction theory for tropical cyclones. Part I: Steady-state maintenance. *J. Atmos. Sci.* **43**: 585–604.

Emanuel KA. 1988. The maximum intensity of hurricanes. *J. Atmos. Sci.* **45**: 1143–1155.

Emanuel KA. 1995. Sensitivity of tropical cyclones to surface exchange coefficients and a revised steady-state model incorporating eye dynamics. *J. Atmos. Sci.* **52**: 3969–3976.

Emanuel KA. 2005. Increasing destructiveness of tropical cyclones over the past 30 years. *Nature* **436**: 686–688.

Frank WM, Ritchie EA. 2001. Effects of vertical wind shear on the intensity and structure of numerically simulated hurricanes. *Mon. Weather Rev.* **129**: 2249–2269.

Houze RA, Chen SS, Smull BF, Lee W-C, Bell MM. 2007. Hurricane intensity and eyewall replacement. *Science* **315**: 1235–1239.

Knutson TK, Tuleya RE. 2004. Impact of CO_2-induced warming on simulated hurricane intensity and precipitation: Sensitivity to the choice of climate model and convective parameterization. *J. Climatol.* **17**: 3477–3495.

Marks FD, Black PG, Montgomery MT, Burpee RW. 2008. Structure of the eye and eyewall of hurricane Hugo (1989). *Mon. Weather Rev.* **136**: 1237–1259.

Montgomery MT, Snell HD, Yang Z. 2001. Axisymmetric spindown dynamics of hurricane-like vortices. *J. Atmos. Sci.* **58**: 421–435.

Montgomery MT, Vladimirov VA, Denissenko PV. 2002. An experimental study on hurricane mesovortices. *J. Fluid Mech.* **471**: 1–32.

Montgomery MT, Bell MM, Aberson SD, Black ML. 2006. Hurricane Isabel (2003): New insights into the physics of intense storms. Part I – Mean vortex structure and maximum intensity estimates. *Bull. Am. Meteorol. Soc.* **87**: 1335–1347.

Nguyen SV, Smith RK, Montgomery MT. 2008. Tropical cyclone intensification and predictability in three dimensions. *Q. J. R. Meteorol. Soc.* **134**: 565–584.

Ooyama KV. 1969. Numerical simulation of the life-cycle of tropical cyclones. *J. Atmos. Sci.* **26**: 3–40.

Persing J, Montgomery MT. 2003. Hurricane superintensity. *J. Atmos. Sci.* **60**: 2349–2371.

Schubert WH, Montgomery MT, Taft RK, Guinn TA, Fulton SR, Kossin JP, Edwards JP. 1999. Polygonal eyewalls, asymmetric eye contraction and potential vorticity mixing in hurricanes. *J. Atmos. Sci.* **56**: 1197–1223.

Smith RK. 1968. The surface boundary layer of a hurricane. *Tellus* **20**: 473–483.

Smith RK. 2000. The role of cumulus convection in hurricanes and its representation in hurricane models. *Rev. Geophys.* **38**: 465–489.

Smith RK. 2003. A simple model of the hurricane boundary layer. *Q. J. R. Meteorol. Soc.* **129**: 1007–1027.

Smith RK, Vogl S. 2008. A simple model of the hurricane boundary layer revisited. *Q. J. R. Meteorol. Soc.* **134**: 337–351.

Smith RK, Montgomery MT, Zhu H. 2005. Buoyancy in tropical cyclones and other rapidly rotating vortices. *Dyn. Atmos. Oceans* **40**: 189–208.

Terwey WD, Montgomery MT. 2008. Secondary eyewall formation in two idealized, full-physics modeled hurricanes. *J. Geophys. Res.* in press.